energies

MDPI

Article

State Estimation of Permanent Magnet Synchronous Motor Using Improved Square Root UKF

Bo Xu [1], Fangqiang Mu [1], Guoding Shi [1], Wei Ji [2,*] and Huangqiu Zhu [1]

[1] The School of Electrical and Information Engineering, Jiangsu University, Zhenjiang 212013, China; xubo@ujs.edu.cn (B.X.); mfqjsdx@163.com (F.M.); sgd18260622040@163.com (G.S.); zhuhuangqiu@ujs.edu.cn (H.Z.)

[2] Key Laboratory of Facility Agriculture Measurement and Control Technology and Equipment of Machinery Industry, Jiangsu University, Zhenjiang 212013, China; jwhxb@163.com

* Correspondence: jwhxb@163.com; Tel.: +86-138-6244-5908

Academic Editor: K. T. Chau

Received: 9 April 2016; Accepted: 20 June 2016; Published: 24 June 2016

Abstract: This paper focuses on an improved square root unscented Kalman filter (SRUKF) and its application for rotor speed and position estimation of permanent magnet synchronous motor (PMSM). The approach, which combines the SRUKF and strong tracking filter, uses the minimal skew simplex transformation to reduce the number of the sigma points, and utilizes the square root filtering to reduce computational errors. The time-varying fading factor and softening factor are introduced to self-adjust the gain matrices and the state forecast covariance square root matrix, which can realize the residuals orthogonality and force the SRUKF to track the real state rapidly. The theoretical analysis of the improved SRUKF and implementation details for PMSM state estimation are examined. The simulation results show that the improved SRUKF has higher nonlinear approximation accuracy, stronger numerical stability and computational efficiency, and it is an effective and powerful tool for PMSM state estimation under the conditions of step response or load disturbance.

Keywords: permanent magnet synchronous motor; square root unscented Kalman filter; state estimation

1. Introduction

The extended Kalman filter (EKF) has been successfully implemented as a state observer for induction motor (IM) drives in various areas [1–8]. However, EKF needs to calculate the nonlinear equation of the Jacobian matrix, which is sub-optimal and can easily lead to divergence. In Ref. [9], Unscented Kalman filter yielded performance equivalent to the Kalman filter for linear systems, yet generalized elegantly to nonlinear systems without the linearization steps required by the EKF. Also in this paper, a symmetric sigma point solution, which used $2n + 1$ points to match the mean and covariance of an n-dimensional random variable, was presented. With this set of points, the unscented transform guaranteed the same performance as the truncated second order filter, with the same order of calculations as an EKF but without the need to calculate any approximations or derivatives. In real-time applications, it is critical that both the computational costs and storage requirements are minimized. In [10], the minimal skew simplex points were introduced, which used the minimum number of sigma points, and reduced the computation time. In [11], UKF was used to estimate the synchronous generator state. Compared with EKF, this method can effectively improve the precision of state estimation. However, covariance asymmetry and non-positive definite defects all exist in both EKF and UKF. A square root unscented Kalman filter (SRUKF) algorithm solves the problem of filtering divergence caused by non-positive of error covariance matrix in general EKF and UKF, and the stability of the algorithm is improved. In [12], SRUKF was used to estimate the speed and rotor

space of permanent magnet synchronous motor, and effectively overcame the numerical calculation defects. The problems of bad robustness for the model parameter change, slow convergence, and lower tracking ability to abrupt state still exist. Strong tracking filter (STF) can adjust the state prediction error covariance matrix and filter gain matrix, which also has a strong robustness of the model mismatch and a unique strong tracking ability. It can effectively improve the tracking performance at a steady and abrupt state [13].

Combining the ordinary SRUKF and strong tracking filtering, this paper presents an improved SRUKF for rotor speed estimation of permanent magnet synchronous motor (PMSM) sensorless drives. On the one hand, the time-varying fading factor and softening factor based on STF theory are introduced to self-adjust the gain matrices and the state forecast covariance square root matrix, which can realize the residuals orthogonality and force the SRUKF track the real state rapidly. On the other hand, Cholesky and QR decomposition are introduced in SRUKF, which can effectively avoid filter divergence caused by the error covariance matrix negative, and improve the convergence speed and stability. The vector control system for PMSM without a speed sensor is set up based on this approach. Rotor position and speed estimators are designed by this method. Simulation results confirm the validity of the proposed approach.

This paper is organized as follows. Section 2 presents the SRUKF. Section 3 discusses the design of improved SRUKF. The PMSM model and observer are described in Section 4, and Section 5 shows the simulation results. Conclusions and future work are given in Section 6.

2. Square-Root UKF

Consider the following a general discrete-time nonlinear dynamic system:

$$\begin{cases} x_{k+1} = f(x_k, u_k) + w_k \\ y_k = h(x_k, u_k) + v_k \end{cases} \tag{1}$$

where $f(,)$ and $h(,)$ denote the nonlinear function with one-order continuous partial derivative. x_k represents the unobserved state of the system. u_k is a known exogenous input. y_k is the observed measurement signal. w_k and v_k are uncorrelated from each other with zero-mean and covariance, respectively. Q_k and R_k are the noise covariance of the process and measurement, respectively.

2.1. The Minimal Skew Simplex Points

The minimal skew sigma points are a simplex set, which is chosen to match the mean, covariance and minimize their skew. These points have the important property that they can be constructed recursively. The point selection algorithm for the simplex unscented transform is as follows:

(1) Choose the initial weight value:

$$0 \leqslant W_0 \leqslant 1 \tag{2}$$

(2) Choose weight sequence:

$$W_i = \begin{cases} \frac{1-W_0}{2^n} & \text{for } i = 1 \\ W_1 & \text{for } i = 2 \\ 2^{i-1} W_1 & \text{for } i = 3, \ldots, n+1 \end{cases} \tag{3}$$

(3) Initialize the vector sequences of sigma points as:

$$\chi_0^1 = [0], \ \chi_1^1 = [-\frac{1}{\sqrt{2W_1}}] \text{ and } \chi_2^1 = [\frac{1}{\sqrt{2W_1}}] \tag{4}$$

(4) Expand vector sequences for $j = 2, \ldots, n$, according to:

$$\chi_i^{j+1} = \begin{cases} \begin{bmatrix} \chi_0^j \\ 0 \end{bmatrix} & \text{for } i = 0 \\ \begin{bmatrix} \chi_i^j \\ -\frac{1}{\sqrt{2W_j}} \end{bmatrix} & \text{for } i = 1, \ldots, j \\ \begin{bmatrix} 0_j \\ \frac{1}{\sqrt{2W_j}} \end{bmatrix} & \text{for } i = j+1 \end{cases} \tag{5}$$

2.2. Square-Root UKF for State-Estimation

The square-root UKF makes use of three powerful linear algebra techniques, QR decomposition, Cholesky factor updating and efficient least squares. The algorithmic description of SRUKF is as follows [12]:

(1) Initialize with

$$\hat{x}_0 = E[x_0] \tag{6}$$

$$P_0 = E[(x_0 - \hat{x}_0)(x_0 - \hat{x}_0)^T] \tag{7}$$

$$S_0 = chol\ (P_0) \tag{8}$$

where $\hat{x}_0$ denotes an initial guess for the initial state x_0, and P_0 is the initial estimation variance. *Chol* $(\cdot)$ represents the matrix square-root using lower triangle Cholesky decomposition.

(2) Sigma point calculation and time update

$$\chi_{k-1} = \hat{x}_{k-1} + S_{k-1}\chi_{k-1} \tag{9}$$

$$\hat{\chi}_{k/k-1} = f(\chi_{i,k-1}, u_{k-1}) \tag{10}$$

$$\hat{x}_k = \sum_{i=0}^{2n} W_i^{(m)} \hat{\chi}_{i,k/k-1} \tag{11}$$

$$S_k^- = qr\left\{[\sqrt{W_1^{(c)}}(\hat{\chi}_{1:2n,k/k-1} - \hat{x}_k)\ \sqrt{Q_k}]\right\} \tag{12}$$

$$S_k = cholupdate\ \left\{S_k^-, \hat{\chi}_{0,k} - \hat{x}_k, W_0^{(c)}]\right\} \tag{13}$$

where $qr\{\cdot\}$ and $cholupdate\{\cdot\}$ represents QR decomposition and Cholesky factor updating.

$$\hat{y}_{k/k-1} = h(\hat{\chi}_{k/k-1}) \tag{14}$$

$$y_k^- = \sum_{i=0}^{2n} W_i^{(m)} \hat{y}_{k/k-1} \tag{15}$$

(3) Measurement update

$$S_{y_k^-} = qr\left\{[\sqrt{W_1^{(c)}}[\hat{y}_{1:2n,k} - y_k^-]\ \sqrt{R_k}]\right\} \tag{16}$$

$$S_{y_k} = cholupdate\left\{[S_{y_k^-}, \hat{y}_{0,k} - y_k^-, W_0^{(c)}]\right\} \tag{17}$$

$$P_{x_k y_k} = \sum_{i=0}^{2n} W_i^{(c)}\{\hat{\chi}_{i,k/k-1} - \hat{x}_k\}\{\hat{y}_{i,k/k-1} - y_k^-\}^T \tag{18}$$

$$K_{k/k} = P_{x_k y_k} {P_{y_k}}^{-1} = (P_{x_k y_k}/S_{y_k}^T)/S_{y_k} \tag{19}$$

$$\hat{x}_{k/k} = \hat{x}_k + K_k[y_k - y_k^-] \tag{20}$$

$$S_k = cholupdate\left\{S_k, K_{k/k}S_{y_k}, -1\right\} \tag{21}$$

3. Improved SRUKF

SRUKF has the benefit of numerical stability, but this method still has bad robustness, slow tracking capacity, and low convergence to the model parameters variation and abrupt state. So, combined with strong tracking filter, improved SRUKF filtering algorithm is presented. The orthogonality conditions, which can make the SRUKF filter become a strong tracking filter [14], are given as follows:

$$E[x_k - \hat{x}_{k/k}][x_k - \hat{x}_{k/k}]^T = MIN \tag{22}$$

$$E[\gamma_{k+j}\gamma_k{}^T] = 0 \tag{23}$$

where *MIN* in Equation (22) means the minimum mean square error and $\gamma_k = y_k - y_k^-$.

SRUKF can satisfy the requirements of Equation (22). In order to satisfy Equation (23), selection principle of the gain matrix $K_{k/k}$ is deduced.

Lemma 1. *Define* $\varepsilon(k) = x_k - \hat{x}_k$, $\hat{x}_k$ *is the estimated state with the improved SRUKF algorithm, if* $O[|\varepsilon(k)|^2] << O[|\varepsilon(k)|]$, *then the following equation exist*.

$$\begin{array}{c} E(\gamma_{k+j}\gamma_k{}^T) \approx H(\hat{x}_{k+j/k+j-1})F(u_{k+j-1}, \hat{x}_{k+j-1/k+j-1})\times \\ (I - K_{k+j-1}H_{k+j-1})F(u_{k+j-2}, \hat{x}_{k+j-1/k+j-2}) \times \ldots \times \\ (I - K_{k+1}H_{k+1})F(u_k, \hat{x}_{k/k})(P_{x_k y_k} - K_{k/k}C_k) \end{array} \tag{24}$$

where $C_k = E(\gamma_k\ \gamma_k{}^T)$. H and F are Jacobian matrixs of $h(k, x_k)$ and $f(k, x_k, u_k)$, respectively.

Proof of Lemma 1.

$$\begin{array}{ll} E(\gamma_{k+j}\gamma_k{}^T) = & E[(y_{k+j} - y_{k+j}^-)\gamma_k{}^T] \\ = & E\{[y_{k+j} - \sum_{i=0}^{2n} W_i^{(m)} h(\hat{\chi}_{k+j/k+j-1})]\gamma_k^T\} \\ \approx & E\{[H(\hat{x}_{k+j/k+j-1})(x_{k+j} - \sum_{i=0}^{2n} W_i^{(m)}\hat{\chi}_{k+j/k+j-1}]\gamma_k^T\} \\ \approx & E\{[H(\hat{x}_{k+j/k+j-1})(x_{k+j} - \hat{x}_{k+j/k+j-1})]\gamma_k{}^T\} \\ \approx & E\{[H(\hat{x}_{k+j/k+j-1})(F(u_{k+j-1}, \hat{x}_{k+j-1/k+j-1}) \times (x_{k+j-1} - \hat{x}_{k+j-1/k+j-1}) + w_{k+j-1})]\gamma_k{}^T\} \\ \approx & E\{[H(\hat{x}_{k+j/k+j-1})(F(u_{k+j-1}, \hat{x}_{k+j-1/k+j-1}) \times (x_{k+j-1} - \hat{x}_{k+j-1/k+j-2} - K_{k+j-1}H_{k+j-1})\times \\ & (x_{k+j-1} - \hat{x}_{k+j-1/k+j-2})]\gamma_k{}^T\} \\ \approx & E\{[H(\hat{x}_{k+j/k+j-1})(F(u_{k+j-1}, \hat{x}_{k+j-1/k+j-1}) \times (I - K_{k+j-1}H_{k+j-1})(x_{k+j-1} - \hat{x}_{k+j-1/k+j-2})\gamma_k{}^T\} \\ \approx & E\{[H(\hat{x}_{k+j/k+j-1})F(u_{k+j-1}, \hat{x}_{k+j-1/k+j-1}) \times (I - K_{k+j-1}H_{k+j-1})F(u_{k+j-2}, \hat{x}_{k+j-1/k+j-2}) \times \ldots \times \\ & (I - K_{k+1}H_{k+1})F(u_k, \hat{x}_{k/k})(x_k - \hat{x}_{k/k})]\gamma_k^T\} \\ \approx & [H(\hat{x}_{k+j/k+j-1})F(u_{k+j-1}, \hat{x}_{k+j-1/k+j-1}) \times (I - K_{k+j-1}H_{k+j-1})F(u_{k+j-2}, \hat{x}_{k+j-1/k+j-2}) \times \ldots \times \\ & (I - K_{k+1}H_{k+1})F(u_k, \hat{x}_{k/k})]E[(x_k - \hat{x}_{k/k})\gamma_k^T] \end{array} \tag{25}$$

where

$$\begin{aligned} E[(x_k - \hat{x}_{k/k})\gamma_k{}^T] &= E[(x_k - \hat{x}_{k/k-1} - K_{k/k}\gamma_k)(y_k - y_k^-)^T] \\ &= E[(x_k - \hat{x}_{k/k-1})(y_k - y_k^-)^T - K_{k/k}\gamma_k\gamma_k{}^T] \\ &= P_{x_k y_k} - K_{k/k}C_k \end{aligned}$$

So Lemma 1 is satisfied. In the proof, the noise and signal is statistical independence, and the three times and above error are ignored.

In order to weaken the effect of old data, and achieve fast tracking to the abrupt status, time-varying fading factor λ_k is introduced as follows

$$K_{k/k} = P_{x_k y_k}(\lambda_k P_{y_k})^{-1} \tag{26}$$

where $\lambda_k = \begin{cases} \lambda_k, & \lambda_k > 1 \\ 1, & \lambda_k \leqslant 1 \end{cases}$.

From Lemma 1, if $P_{x_k y_k} - K_{k/k} C_k = 0$, i.e., $I - (\lambda_k P_{y_k})^{-1} C_k = 0$, then the following equation can be deduced.

$$\lambda_k S_{y_k} S_{y_k}^T = C_k \tag{27}$$

Solving the trace of Equation (27),

$$tr(\lambda_k S_{y_k} S_{y_k}^T) = tr C_k \tag{28}$$

In order to avoid excessive regulation of λ_k, and achieve more smooth of the state estimation, softening factor η is introduced, then Equation (28) becomes

$$\lambda_k = \frac{tr(C_k - \eta R_k)}{tr(S_{y_k} S_{y_k}^T)} \tag{29}$$

where $C_k = \begin{cases} \gamma_0 \gamma_0^T & k = 0 \\ \frac{\rho C_{k-1} + \gamma_k \gamma_k^T}{1+\rho} & k \geqslant 1 \end{cases}$, ρ is forgetting factor, $0 < \rho \leqslant 0.95$. Generally, $\rho = 0.95$. When the model is more accurate, $\lambda_k = 1$, the improved SRUKF degrades into SRUKF.

4. Mathematical Model of PMSM and System Implementation

4.1. Mathematical Model of PMSM

The mathematical model of PMSM in α–β coordinate system can be represented as follows

$$\begin{bmatrix} \frac{di_\alpha}{dt} \\ \frac{di_\beta}{dt} \\ \frac{d\omega}{dt} \\ \frac{d\theta}{dt} \end{bmatrix} = \begin{bmatrix} -\frac{R}{L_d} i_\alpha + \frac{\psi_f}{L_d} P_1 \omega \sin\theta \\ -\frac{R}{L_q} i_\beta - \frac{\psi}{L_q} P_1 \omega \cos\theta \\ \frac{1}{J}(T_e - F\omega - T_m) \\ P_1 \omega \end{bmatrix} + \begin{bmatrix} \frac{1}{L_d} & 0 \\ 0 & \frac{1}{L_d} \\ 0 & 0 \\ 0 & 0 \end{bmatrix} \cdot \begin{bmatrix} u_\alpha \\ u_\beta \end{bmatrix} \tag{30}$$

$$y = \begin{bmatrix} i_\alpha & i_\beta \end{bmatrix}^T = \begin{bmatrix} 1 & 0 & 0 & 0 \\ 0 & 1 & 0 & 0 \end{bmatrix} \cdot \begin{bmatrix} i_\alpha \\ i_\beta \\ \omega \\ \theta \end{bmatrix} \tag{31}$$

where u_α, u_β and i_α, i_β are the stator voltage and current respectively. Ψ_f is magnet flux linkage. L_d and L_q are the stator inductance in d–q coordinate system, respectively. F is the friction coefficient of rotor and load. R is the stator resistance. T_e and T_m are the electromagnetic torque and mechanical torque, respectively. P_1 is the number of pole pairs in torque winding. J is the total moment of inertia of the mechanical system. θ is the angle of rotor position. ω is the rotor speed. Assuming the sampling period T_s, the Equations (30) and (31) are discretized. We set the state variable $\boldsymbol{X}_k = [i_{1\alpha,k}\ i_{1\beta,k}\ \omega_k\ \theta_k]^{\mathrm{T}}$, control variables $\boldsymbol{U}_k = [u_{1\alpha,k}\ u_{1\beta,k}]^{\mathrm{T}}$, output variables $\boldsymbol{Y}_k = [i_{1\alpha,k}\ i_{1\beta,k}]^{\mathrm{T}}$. From the discretization Formula (32),

$$\dot{\mathbf{X}} \approx \frac{1}{T_\mathrm{s}}(\mathbf{X}_{k+1} - \mathbf{X}_k) \tag{32}$$

Equations (30) and (31) can be transformed to

$$\mathbf{X}_{k+1} = \begin{bmatrix} i_{\alpha,k+1} \\ i_{\beta,k+1} \\ \omega_{k+1} \\ \theta_{k+1} \end{bmatrix} = \begin{bmatrix} (1 - T_\mathrm{s}\frac{R}{L_\mathrm{d}}) i_{\alpha,k} + T_\mathrm{s}\frac{\psi_\mathrm{f}}{L_\mathrm{d}} P_1 \omega_k \sin\theta_k \\ (1 - T_\mathrm{s}\frac{R}{L_\mathrm{q}}) i_{\beta,k} - T_\mathrm{s}\frac{\psi_\mathrm{f}}{L_\mathrm{q}} P_1 \omega_k \cos\theta_k + \begin{bmatrix} \frac{T_\mathrm{s}}{L_d} & 0 \\ 0 & \frac{T_\mathrm{s}}{L_d} \\ 0 & 0 \\ 0 & 0 \end{bmatrix} \cdot \begin{bmatrix} u_{\alpha,k} \\ u_{\beta,k} \end{bmatrix} \\ (1 - \frac{T_\mathrm{s}}{J} F)\omega_k + \frac{T_\mathrm{s}}{J}(T_\mathrm{e} - T_\mathrm{m}) \\ T_\mathrm{s} P_1 \omega_k + \theta_k \end{bmatrix} \tag{33}$$

$$\mathbf{Y}_k = \begin{bmatrix} i_{\alpha,k} & i_{\beta,k} \end{bmatrix}^{\mathrm{T}} = \begin{bmatrix} 1 & 0 & 0 & 0 \\ 0 & 1 & 0 & 0 \end{bmatrix} \cdot \begin{bmatrix} i_{\alpha,k} \\ i_{\beta,k} \\ \omega \\ \theta \end{bmatrix} \tag{34}$$

$$\mathbf{H}_k = \begin{bmatrix} 1 & 0 & 0 & 0 \\ 0 & 1 & 0 & 0 \end{bmatrix} \tag{35}$$

4.2. System Implementation

The basic configuration of speed sensorless vector control system for PMSM based on the improved SRUKF is shown in Figure 1. The space vector pulse width modulation (SVPWM) inverter is used. Parameters of PMSM used in simulation experiment are shown in Table 1.

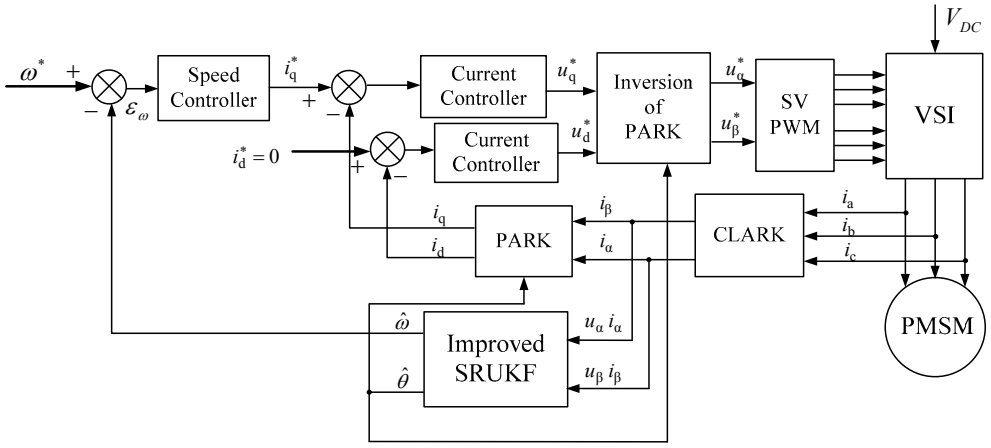

Figure 1. Configuration of the vector control system based on improved SRUKF.

Table 1. Parameter of PMSM.

Parameter	Symbol	Value
Number of poles pairs in torque winding	P_1	4
Stator resistance	R	4.025 Ω
d-axis inductance	L_d	11.9 mH
q-axis inductance	L_q	11.9 mH
Magnet flux linkage	ψ_f	0.245 Wb
Rotor inertia	J	1.0×10^{-4} kg· m^2
Rotor mass	m	1.2 kg
Rated voltage of torque winding	V	240 V
Rated current	I	5.86 A
The maximum electromagnetic torque	T_e	18.82 N· m
Mechanical time constant	T	0.25 s
Rated load torque	T_m	9.41 N· m
Speed range	ω	0–1000 rad/s

The simulation solver mode is ode3 with fixed step. Simulation time is 0.1s. The following values are chosen in simulation: $x_0 = 0$, $P_0 = diag(0.2, 0.2, 180, 20)$, $W_0 = 0.25$, $Q_k = diag(10^{-6}, 10^{-6}, 10^{-2}, 10^{-5})$, $R_k = diag(0.1, 0.1)$, $\eta = diag(3.2, 3.2)$.

5. Simulation Results and Error Analysis

5.1. Simulation Results

The performance of the improved SRUKF observer is validated subject to a speed command. Experimental results are shown in Figures 2–16. In which, "Real" indicates the measurement speed, "SRUKF", and "improved SRUKF" indicate the speed or space position estimation and error with

the SRUKF and improved SRUKF, respectively. $\Delta\theta=\theta-\hat{\theta}$, θ is the measurement space position of the rotor, $\hat{\theta}$ is the estimation space position, $\Delta\theta$ is the space position estimation error. In Figure 2, the rotor speed ω reference is 50 rad/s, during this test, the motor is loaded at 3 N·m. The estimated and measured speeds match well, which indicates that the observer provides a good estimate at low speeds. The corresponding space position estimation and error are shown in Figures 3 and 4. The error of improved SRUKF is smaller than SRUKF.

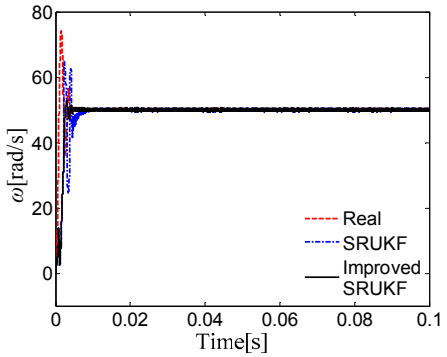

Figure 2. Speed estimation at 50 rad/s.

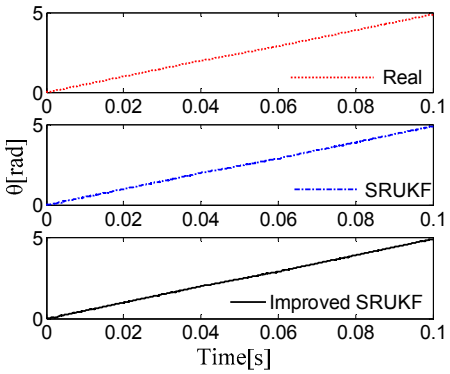

Figure 3. Space position estimation at 50 rad/s.

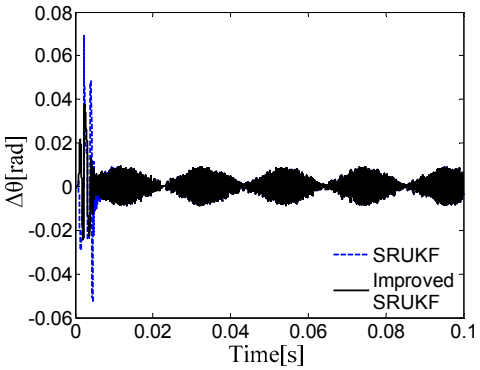

Figure 4. Space position estimation error at 50 rad/s.

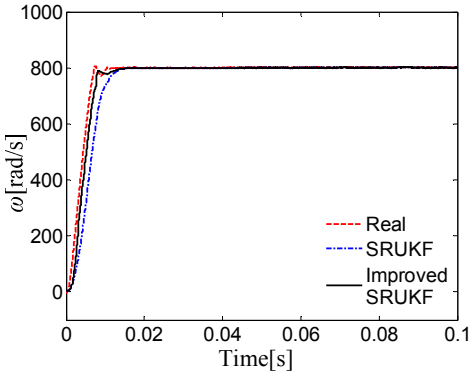

Figure 5. Speed estimation at 800 rad/s.

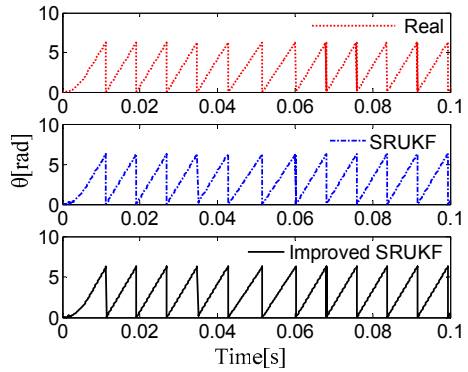

Figure 6. Space position estimation at 800 rad/s.

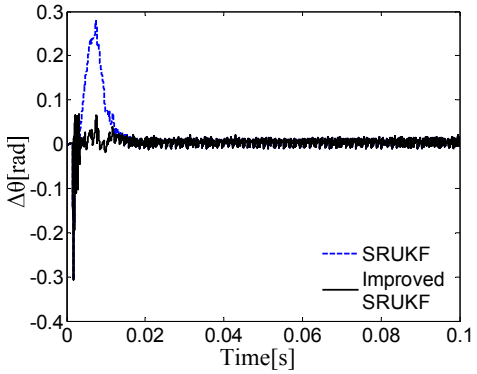

Figure 7. Space position estimation error at 800 rad/s.

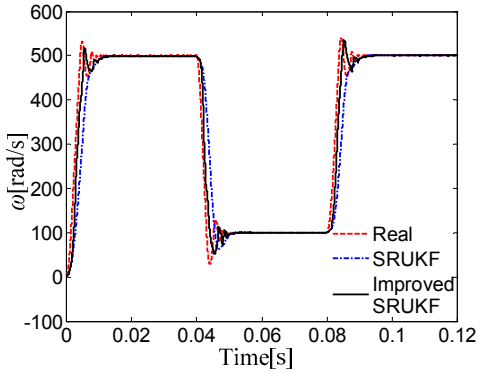

Figure 8. Speed estimation at speed step response.

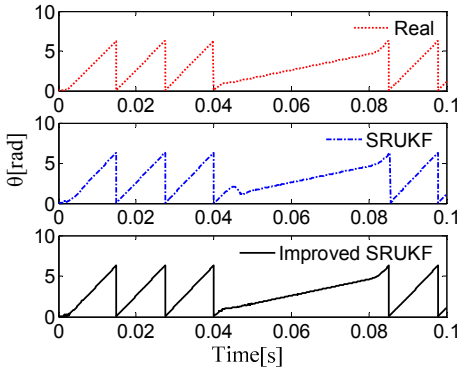

Figure 9. Space position estimation at speed step response.

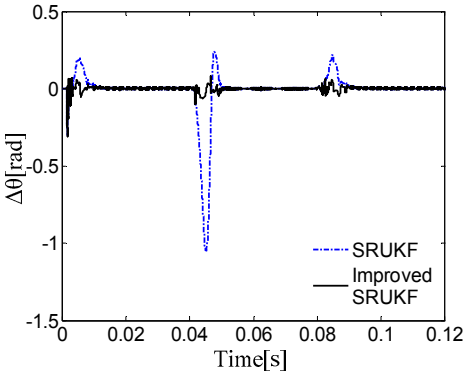

Figure 10. Space position estimation error at speed step response.

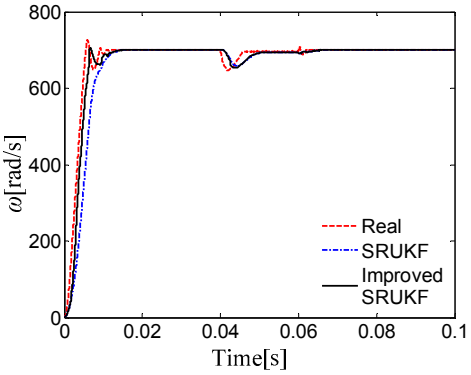

Figure 11. Speed estimation at load disturbance.

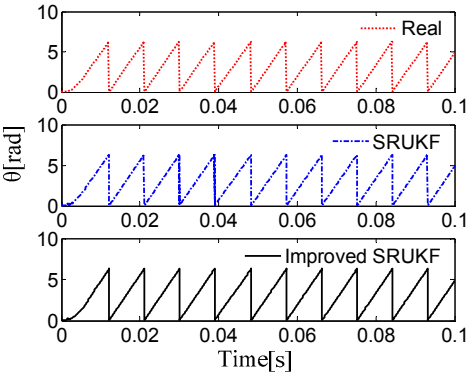

Figure 12. Space position estimation at load disturbance.

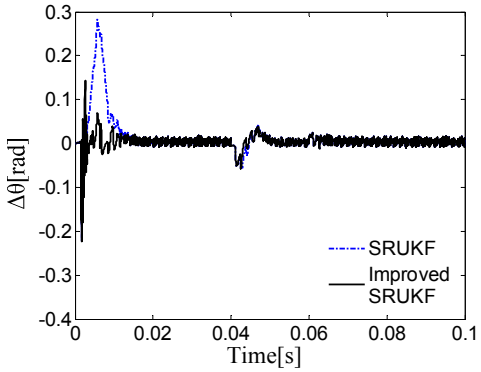

Figure 13. Space position estimation error at load disturbance.

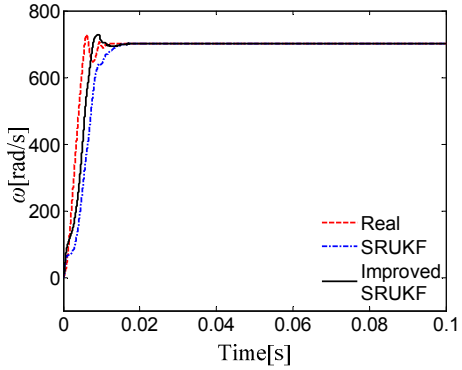

Figure 14. Speed estimation at parameters disturbance.

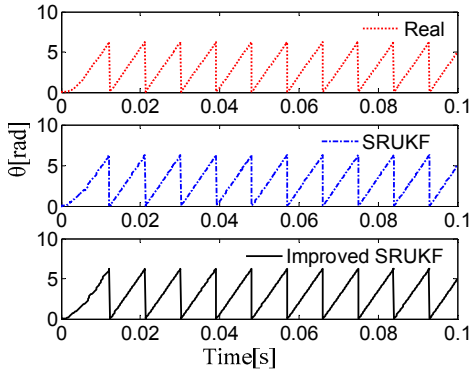

Figure 15. Space position estimation error at parameters disturbance.

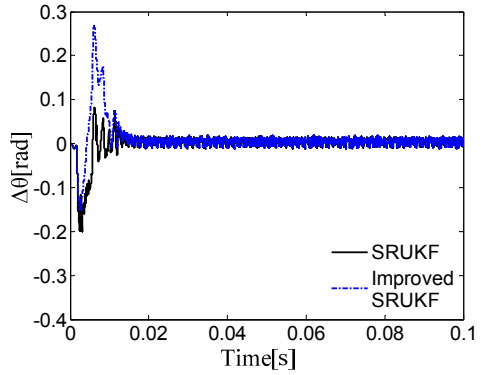

Figure 16. Space position estimation error at parameters disturbance.

In Figure 5, the drive runs at a reference speed of 800 rad/s. In Figure 8, the reference speed is 500 rad/s. The reference speed is abruptly changed to 100 rad/s at 0.04 s, and then, the reference speed is abruptly returned to 500 rad/s. In Figure 11, the drive runs at a reference speed of 700 rad/s, the disturbance is loaded at 0.04 s–0.06 s. The corresponding space position estimation and error are shown in Figures 6, 7, 9, 10, 12 and 13, respectively.

Considering the change of motor physical parameters during PMSM operation, approximate parameter values are used in the observer. Waveforms for operation with detuned stator and rotor resistances are shown in Figures 14–16, respectively. The stator resistance and d, q axis inductance are detuned by increasing 25%, with respect to the values in the Table 1. The results show that the observer remains stable and can handle well.

The experimental results show that the estimated speed follows the actual speed closely with rapid dynamics, and small estimation error of rotor space is achieved. It indicates that the improved SRUKF is an accurate and fast state estimator. Also, compared with the ordinary SRUKF, the improved SRUKF exhibits a strong robustness and estimation accuracy under the conditions of step response or load disturbance.

5.2. Error Analysis

Set the root mean square error (RMSE) as the system estimation quality evaluation criteria

$$RMSE(x) = \sqrt{E[|x - \hat{x}|^2]} = \sqrt{\frac{1}{N}\sum_{i=1}^{N}|x - \hat{x}|^2} \tag{36}$$

where x is the actual measurement. $\hat{x}$ is an estimation. N is the sampling number.

Tables 2 and 3 show the RMSE of speed estimation and rotor space position estimation, respectively. From the tables, it can be found that system performance is little difference between SRUKF and improved SRUKF under the conditions of steady state. However, under the conditions of step response or load disturbance, speed estimation error of improved SRUKF reduced about 55% more than SRUKF, and space position estimation error reduced about 65%.

Table 2. RMSE of speed estimation.

Method / Speed	SRUKF	Improved SRUKF
50 rad/s	6.7865	6.1343
800 rad/s	61.4532	25.1143
700 rad/s load disturbance	55.7270	25.3146
500 rad/s to 100 rad/s to 500 rad/s	71.6219	31.5823
parameters disturbance	55.2042	43.0836

Table 3. RMSE of space position estimation.

Method / Speed	SRUKF	Improved SRUKF
50 rad/s	0.0066	0.0053
800 rad/s	0.0511	0.0133
700 rad/s load disturbance	0.0458	0.0156
500 rad/s to 100 rad/s to 500 rad/s	0.1541	0.0187
parameters disturbance	0.1084	0.0451

Figure 17 shows the values of the time-varying fading factor at speed accelerated from 500 rad/s to 100 rad/s, then to 500 rad/s. Figure 18 shows the values of the time-varying fading factor at parameters disturbance. Time-varying fading factor is adaptive, which can adjust the filter gain and

error covariance square root matrix. During steady-state operation at a constant speed, time-varying fading factor equals 1, and the improved SRUKF filter degrades to ordinary SRUKF.

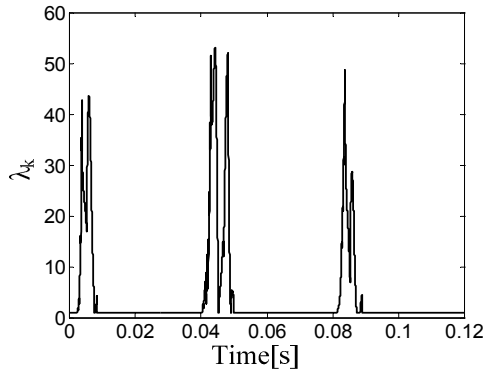

Figure 17. Fading factors of speed step response.

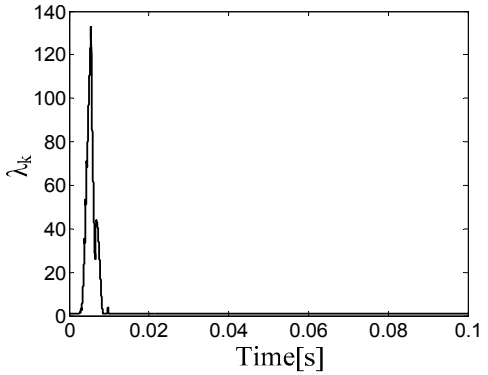

Figure 18. Fading factors of parameters disturbance.

6. Conclusions

This paper has proposed and investigated an improved SRUKF filter for state estimation in sensorless PMSM drives. The main contribution is the combination of the SRUKF and a strong tracking filter. The SRUKF reduces the computational errors by propagating the SR of matrices instead of the matrices themselves. In order to realize the residuals orthogonality and force the SRUKF filter to track the real state rapidly, the time-varying fading factor and softening factor are introduced to self-adjust gain matrices and the state forecast covariance square root matrix.

A speed sensorless vector control system for PMSM based on the improved SRUKF is implemented. The simulation results illustrate that the proposed method has higher nonlinear approximation accuracy, stronger numerical stability, and computational efficiency. Strong robustness is achieved under the conditions of low speed, high speed, step response, and load disturbance. It can achieve a precise estimate of the speed, space position, and ensure the rotor suspends stably. Going forward, learning how to apply this algorithm on an actual system based on DSP will be the next project.

Acknowledgments: This work is supported by Natural Science Foundation of Jiangsu Province (grant number BK20150530), Jiangsu Province Colleges and Universities Natural Science Research Project (grant number 12KJB470002), A Project Funded by the Priority Academic Program Development of Jiangsu Higher Education Institutions (PAPD), and the Professional Research Foundation for Advanced Talents of Jiangsu University (grant number 14JDG077).

Author Contributions: All authors have worked on this manuscript together and all authors have read and approved the final manuscript.

Conflicts of Interest: The authors declare no conflicts of interest.

Nomenclature

P_1	Number of poles pairs in torque winding
R	Stator resistance
L_d (L_q)	Stator inductance in d–q coordinate system
ψ_f	Magnet flux linkage
J	Rotor moment of inertia
M	Rotor mass
V	Rated voltage of torque winding
I	Rated current
T_e	Electromagnetic torque
T	Mechanical time constant
T_m	Rated mechanical torque
T_s	Sampling period
θ	Rotor angle position
ω	Rotor speed
F	Friction coefficient
u_α (u_β)	Stator voltage in α–β coordinate system
i_α (i_β)	Stator current in α–β coordinate system

References

1. Kalman, R.E. A new approach to linear filtering and prediction problems. *J. Basic Eng.* **1960**, *82*, 35–45. [CrossRef]
2. Alonge, F.; D'Ippolito, F.; Sferlazza, A. Sensorless control of induction-motor drive based on robust Kalman filter and adaptive speed estimation. *IEEE Trans. Ind. Electron.* **2014**, *61*, 1444–1453. [CrossRef]
3. Salvatore, N.; Caponio, A.; Neri, F.; Stasi, S.; Cascella, G.L. Optimization of delayed-state Kalman-filter-based algorithm via differential evolution for sensorless control of induction motors. *IEEE Trans. Ind. Electron.* **2010**, *57*, 385–394. [CrossRef]
4. Masi, A.; Butcher, M.; Martino, M.; Picatos, R. An application of the extended Kalman filter for a sensorless stepper motor drive working with long cables. *IEEE Trans. Ind. Electron.* **2012**, *59*, 4217–4225. [CrossRef]
5. Laamari, Y.; Chafaa, K.; Athamena, B. Particle swarm optimization of an extended Kalman filter for speed and rotor flux estimation of an induction motor drive. *Electr. Eng.* **2015**, *97*, 129–138. [CrossRef]
6. Bolognani, S.; Oboe, R.; Zigliotto, M. Sensorless full-digital PMSM drive with EKF estimation of speed and rotor position. *IEEE Trans. Ind. Electron.* **1999**, *46*, 184–191. [CrossRef]
7. Lu, K.Y.; Lei, X.; Blaabjerg, F. Artificial inductance concept to compensate nonlinear inductance effects in the back EMF-based sensorless control method for PMSM. *IEEE Trans. Energy Convers.* **2013**, *28*, 593–600. [CrossRef]
8. Kumar, S.; Prakash, J.; Kanagasabapathy, P. A critical evaluation and experimental verification of Extended Kalman Filter, Unscented Kalman Filter and Neural State Filter for state estimation of three phase induction motor. *Appl. Soft Comput.* **2011**, *11*, 3199–3208. [CrossRef]
9. Julier, J.S.; Uhlmann, J.; Whyte, H.D. A new method for the nonlinear transformation of means and covariance in filters and estimators. *IEEE Trans. Autom. Control* **2000**, *45*, 477–482. [CrossRef]
10. Julier, J.S.; Uhlmann, J. Reduced sigma point filters for the propagation of means and covariances through nonlinear transformations. In Proceedings of the American Control Conference, Anchorage, AK, USA, 8–10 May 2002; pp. 887–892.
11. Ghahremani, E.; Kamwa, I. Online state estimation of a synchronous generator using unscented Kalman filter from phasor measurements units. *IEEE Trans. Energy Convers.* **2011**, *26*, 1099–1108. [CrossRef]
12. Jafarzadeh, S.; Lascu, C.; Fadali, M.S. Square root unscented Kalman filters for state estimation of induction motor drives. *IEEE Trans. Ind. Appl.* **2013**, *49*, 92–99. [CrossRef]

13. He, X.; Wang, Z.D.; Wang, X.F. Networked strong tracking filtering with multiple packet dropouts: Algorithms and applications. *IEEE Trans. Ind. Electron.* **2014**, *61*, 1454–1463. [CrossRef]
14. Zhou, D.H.; Ye, Y.Z. *Modern Fault Diagnosis and Fault-Tolerant Control*; Tsinghua University Press: Beijing, China, 2000.